ACS OMEGA

http://pubs.acs.org/journal/acsodf

Article

Tuning the Photochromism of Spiropyran in Functionalized Nanoporous Silica Nanoparticles for Dynamic Anticounterfeiting Applications

Yuhui Yang,*,‖ Huimin Zhao,‖ Yuqing Li, Yilong Chen, Zhaohui Wang, Wei Wu, Leilei Hu, and Jiangkun Zhu

Cite This: *ACS Omega* 2023, 8, 16459−16470

Read Online

ACCESS | Metrics & More | Article Recommendations | Supporting Information

ABSTRACT: Here, we report a novel invisible ink with different decay times based on thin films with different molar ratios of spiropyran (SP)/Si, which allows the encryption of messages over time. Nanoporous silica has been found to be an excellent substrate to improve the solid photochromism of spiropyran, but the hydroxyl groups of silica have a serious effect on fade speeds. The density of silanol groups in silica has an influence on the switching behavior of spiropyran molecules, as they stabilize the amphiphilic merocyanine isomers and thus slow down the fading process from the open to the closed form. Here, we investigate the solid photochromic behavior of spiropyran by sol−gel modification of the silanol groups and explore its potential application in UV printing and dynamic anticounterfeiting. To extend its applications, spiropyran is embedded in organically modified thin films prepared by the sol−gel method. Notably, by using the different decay times of thin films with different SP/Si molar ratios, time-dependent information encryption can be realized. It provides an initial "false" code, which does not display the required information, and only after a given time will the encrypted data appear.

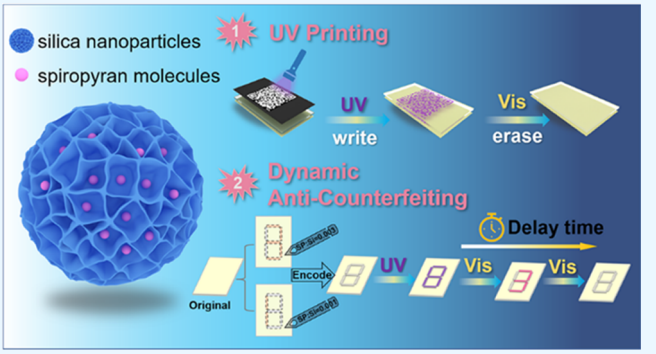

1. INTRODUCTION

Photochromic materials are a class of materials that are able to change color under the irradiation of light, which renders them important candidates for a wide range of practical applications, such as optical switching, information storage, security printing ink, and so on.[1−11] Spiropyran (SP) and its derivatives are essential photochromic compounds because they can be reversibly transformed between states with distinctly different properties (e.g., color and polarity) and their functional properties can be tuned by chemical modification or alteration of the environmental medium.[3,12−16] The photoisomerization of the spiropyrans switches between the colorless spiral ring and the colored merocyanine isomer occurred under light stimulation.[17] In addition, other external stimuli (pH, metal ions, solvent polarity, mechanical forces, etc.) can also promote isomerization.[15,18−25] However, these powerful stimulation-switching abilities work best in soft materials or solutions and have greatly limited their practical application occasion. This phenomenon is mainly caused by two factors: (a) the conversion between the SP form and merocyanine (MC) form of spiropyrans requires a large space, which is hindered in the solid state and (b) strong interactions from the surrounding solid matrix (hydroxyl groups, etc.) may alter their relative energies in different states, which ultimately prevents the direct transfer of the optimal switching properties found in the solution to the final materials. Therefore, one of the main tasks of developing solid-state photoresponsive materials for practical applications is to improve the solid photochromic properties.

One of the leading strategies proposed to avoid this shortcoming is to select substrates with suitable properties to ensure minimal interaction with spiropyran and/or to provide it with sufficient free volume to maintain its solution-like stimulus-sensitive response as well. There are several common methods to achieve this goal, including introducing rigid steric hindrance groups (e.g., polymers or gels) or nanoporous materials (e.g., silica and metal−organic and covalent organic frameworks).[26−34] Especially, using nanoporous materials to load photochromic molecules to improve photochromic properties is a very popular method. Among them, nanoporous host−guest materials are a very attractive substrate for dye dispersion since the large pore volume and high specific surface

Received: March 9, 2023
Accepted: April 13, 2023
Published: April 27, 2023

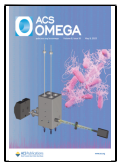

ACS Publications

© 2023 The Authors. Published by American Chemical Society

Scheme 1. Schematic Diagram of the Synthesis Process of NX and NX@SP

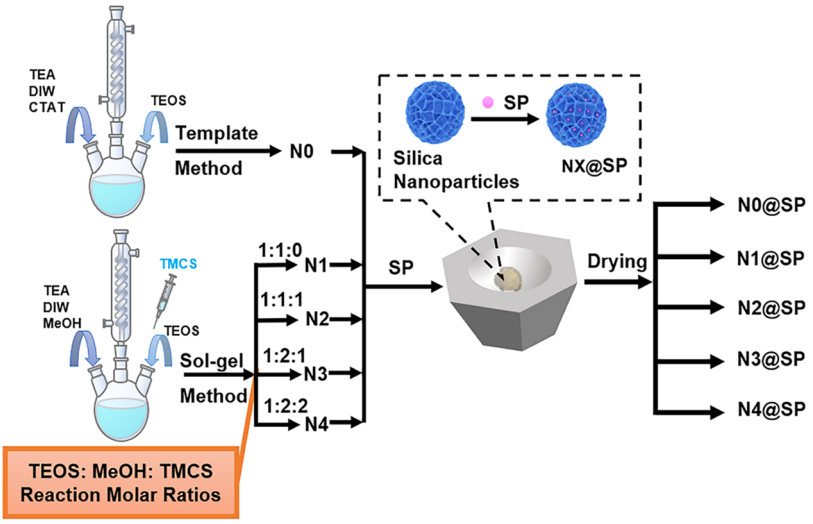

area can accommodate a large amount of dye that is finely dispersed and sufficient for the conversion reaction to work smoothly. Allouche et al.[35] synthesized photochromic hybrid spiropyran−silica nanoparticles with a core−shell structure via the sol−gel procedure, and the silica precursors are tetraethoxysilane (TEOS) and methyltriethoxysilane (MTEOS). Pinto et al.[36] prepared photochromic color-changing silica nanoparticles by covalent immobilization of silylated naphthopyrans or by direct adsorption of parent naphthopyrans onto silica particles for successful application on textiles. Yamaguchi et al.[37] prepared colored hybrids in dendritic fibrous silica based on the composition of nanoporous silica by the adsorption of helical pyran solutions onto nanoporous silica under UV irradiation (photoinduced adsorption), which exhibited a unique negative photochromic behavior in the solid state. However, the challenge in this system is the fade speed is very slow due to the rigid matrix of silica. In addition, the content of silanol groups in the silica matrix wall has an influence on the conversion behavior of spiropyrans as they stabilize spiropyrans in the MC state and thus delay the fading process from the MC to the SP state. This problem has seriously restricted its practical application. As a result, it is necessary to improve the fading rate.

In this paper, we chose to analyze the silanol groups on the light-fading behavior of a typical spiropyran dye encapsulated in functionalized nanoporous silicates. We use trimethylsilyl chloride to modify silanol groups on the walls of silica substrates, and the introduced porous silicate can dramatically reduce the molecular stacking between photochromic compounds, thereby offering enough free volume for efficient SP to MC state photoconversion. We should point out that this work is somewhat similar to Allouche's, but there are also great differences.[35] First, the preparation method is different. They prepare silica with the core−shell structure, and spiropyran molecules are attached by chemical grafting, while we modified spherical silica by the sol−gel method and attached spiropyran by physical adsorption. Although our approaches are different, these two studies both illustrate that the SP-modified materials show the same behavior that photochromic behavior depends on the polarity of the environment and that it does not make a difference if the responsive molecule is chemically grafted or simply physically attached to the silica nanoparticle surface. Second, the reagents are different. They use methyltriethoxysilane, while we use trimethylchlorosilane (TMCS) to modify silanol groups. Third, comparing the content of their studies, we further provide time-dependent information encryption by using the different decay time environments of thin films with different SP/Si molar ratios, which is very useful in our daily life. As we know, in the information age, we are easily exposed to the dangers of information leakage and exposure. It will be particularly important to improve the inevitability of information security protection. In order to push a higher level of encrypted information further, it is important to explore novel methods with additional encryption complexity and unpredictability. Time-dependent message encryption here is to be defined as a system with two readable message states (correct and incorrect) at distinct times, coupled with a blank (completely colorless) nonmessage state, which can provide complex and unpredictable information security guarantees. Especially it should be possible to achieve reinforced cryptographic means by producing a state that offers a misleading/unreadable message at distinct times or by being exposed to the results of different stimuli. Efforts have already been made in this regard. However, up to now, most reports have depended on time-varying cryptographic means, which often rely on associations of multicolored materials with different fluorescent or phosphorescent material characteristics.[38−41] Because the message is usually short-lived during decryption, high-speed photography is often required to monitor it. Alternatively, the duration of the decrypted state can be extended by introducing ultralong room-temperature phosphorescent materials to allow visual observation. Here, we report a novel invisible ink with different decay times based on thin films with different SP/Si molar ratios, which allows the encryption of messages over time.

2. EXPERIMENTAL SECTION

2.1. Synthesis of Modified Silica. The five silica nanoparticles with different densities of silanol groups were prepared by different synthetic methods.[25,41−43] As shown in Scheme 1, during the process of template-based synthesis, TEOS was hydrolytically condensed to give the corresponding silica nanoparticle, which was centrifuged and calcined using cetyl-trimethylammonium tosylate (CTAT) to give N0. Using

https://doi.org/10.1021/acsomega.3c01604
ACS Omega 2023, 8, 16459−16470

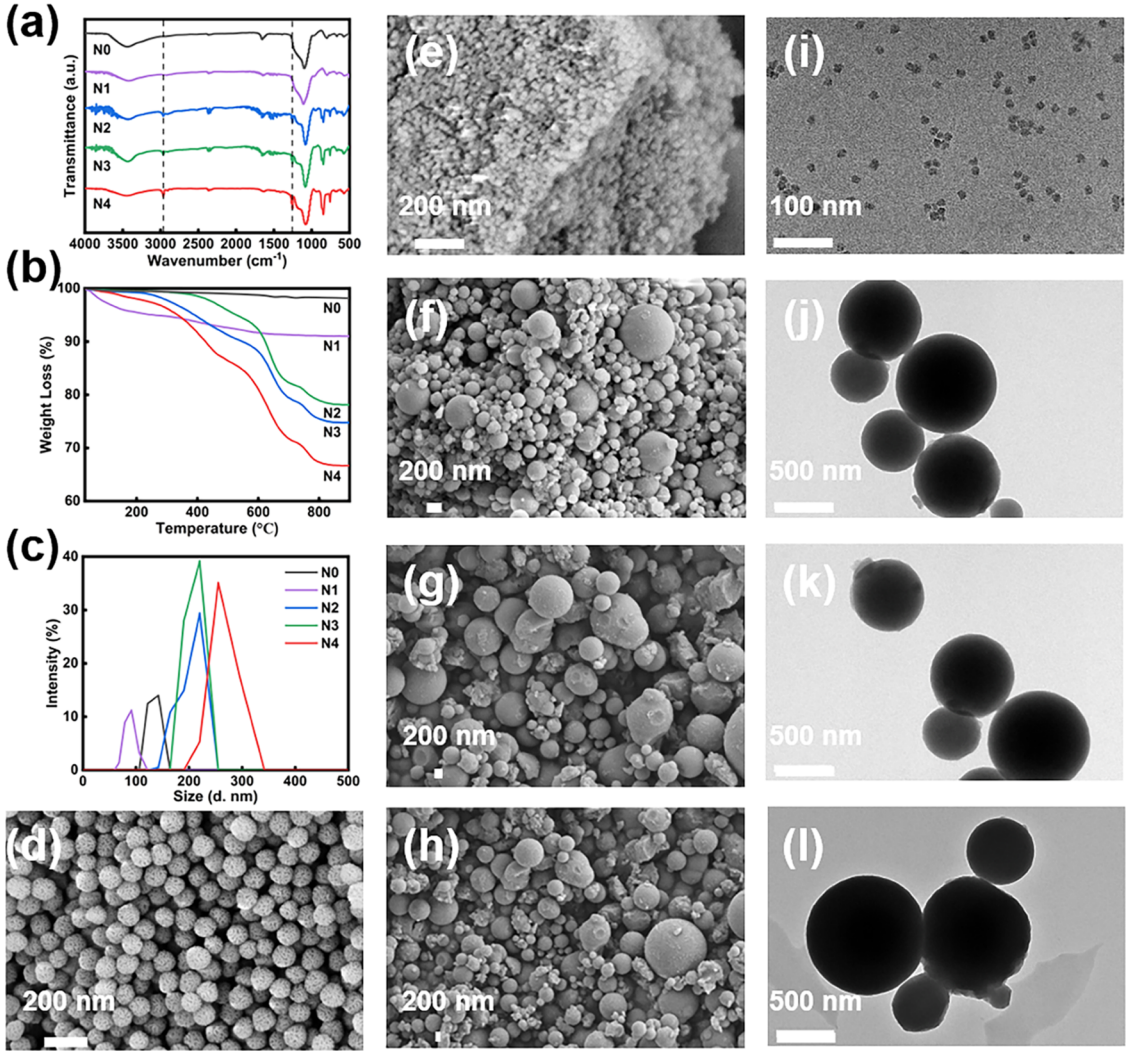

Figure 1. Characterization of modified silica nanoparticles. (a) FT-IR spectra, (b) TGA, and (c) particle size distribution of N0−N4. SEM images of (d) N0, (e) N1, (f) N2, (g) N3, and (h) N4. TEM images of (i) N1, (j) N2, (k) N3, and (l) N4.

TMCS as the functional group reagent and methanol (MeOH) as a cosolvent, the silica nanoparticles were modified with the sol−gel method (also known as the "one-pot method"), and the molar ratio of TEOS/MeOH/TMCS was adjusted to obtain N1−N4. Silica nanoparticles N0−N4 used in this work belong to two classes: N0 and N1 are silica nanoparticles containing only hydroxyl groups, while N2, N3, and N4 are silica nanoparticles with different densities of Si−CH_3 groups. Detailed experimental procedures for the synthesis of these five silica nanoparticles are described in the Supporting Information.

2.2. Preparation of the Photochromic Powder. The key to preparing photochromic powders is to prepare spiropyran molecules and silica nanoparticles having different densities of silanol groups. SP is synthesized using the same procedure as the literature.[18] All photochromic powders are prepared through the solvent evaporation method. First, SP was dissolved in a toluene solution, and the corresponding photochromic solution was obtained by magnetic stirring to completely dissolve it evenly. Then, the final photochromic solution was subsequently added to the previously obtained silica nanoparticles (N0−N4) powder. Successively, the mixture was allowed to evaporate the solvent naturally at room temperature, and uniform adsorption was ensured through constant stirring. The process was repeated for several minutes until the solvent was completely evaporated, and the final photochromic powders were obtained, which were named N0@SP, N1@SP, N2@SP, N3@SP, and N4@SP, respectively. For the sake of simplicity in the later description, NX@SP was used to refer to the five photochromic powders of N0@SP, N1@SP, N2@SP, N3@SP, and N4@SP. The detailed process is described in the Supporting Information.

2.3. Preparation of the Photochromic Film. Photochromic films were prepared by combining SP molecules into a silica matrix using the sol−gel method, which is necessary to prepare the initial sol to obtain a transparent thin film with good optical properties. The introduction of a photochromic dye into such a sol is limited by the low compatibility of the dye in the silica sol. In this sense, we chose a tetrahydrofuran solution, which can not only dissolve spiropyran well but also be evenly distributed in the silica sol.

3. RESULTS AND DISCUSSION

3.1. Characteristics of Modified Silica. To investigate the effect of the density of hydroxyl groups on the photochromic behavior of spiropyran, we prepared a series

https://doi.org/10.1021/acsomega.3c01604
ACS Omega 2023, 8, 16459−16470

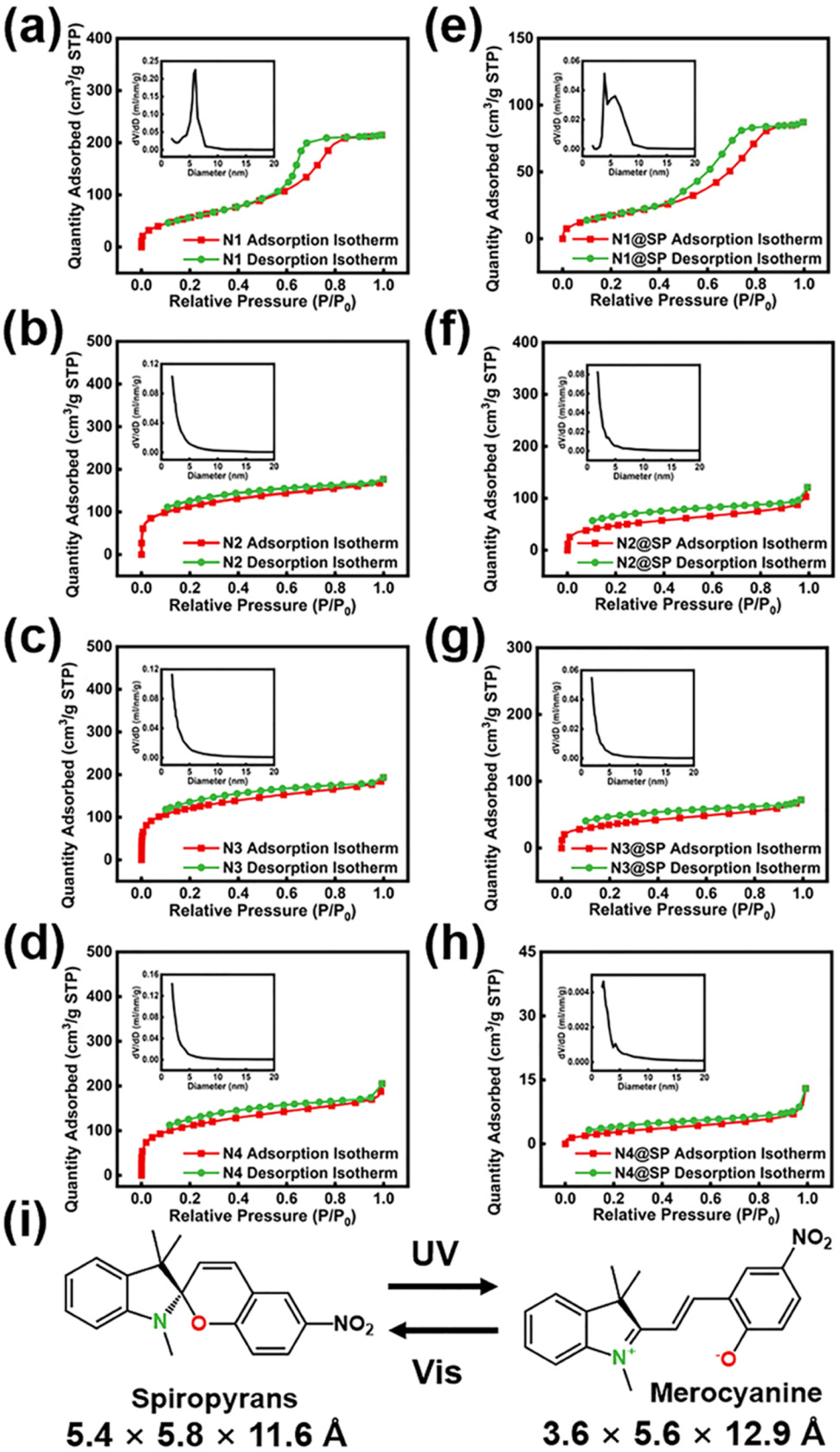

Figure 2. N_2 absorption−desorption isotherms of silica nanoparticles before and after loading: (a) N1, (b) N2, (c) N3, (d) N4, (e) N1@SP, (f) N2@SP, (g) N3@SP, and (h) N4@SP. Inset: the corresponding nanoparticles pore size distributions. (i) Photochromic mechanism of spiropyran and the molecular size of the corresponding form.

https://doi.org/10.1021/acsomega.3c01604
ACS Omega 2023, 8, 16459−16470

of porous silica with different densities of hydroxyl groups. The chemical structure of silica before and after modification was identified by Fourier transform infrared spectroscopy (FT-IR). N0 and N1 have characteristic strong silicon peaks at 1095 and 806 cm^{-1}, corresponding to asymmetric vibrations of the Si−O−Si bond and stretching vibrations of the Si−O bond (Figure 1a). The peak at 3488 cm^{-1} is the formation of Si−OH by hydroxylation, while the peak at 1627 cm^{-1} is associated with the −OH bending vibration of physically adsorbed water. For N2, N3, and N4, the absence of changes in these characteristic peaks indicates that the main structure has not been altered by the modification reaction. In addition, here, some new peaks appear (2960 cm^{-1} belongs to the $-CH_3$ stretching vibration; 1274 cm^{-1} peak belongs to the $Si-CH_3$ vibration), which could indicate that the methyl group was successfully grafted onto the surface of silica.[44,45] These results show that some silanol groups have been successfully transformed into the $Si-CH_3$ group.

To calculate the content of the $Si-CH_3$ group, we executed the thermogravimetric analysis (TGA) test by heating the sample from 30 to 900 °C at a heating rate of 10 °C/min under a nitrogen atmosphere. As can be seen from Figure 1b, the TG curve of N1 has a 4% weight loss until 150 °C, which is mainly due to the evaporation of the methanol solvent. The TG curves of unmodified silica (N0, N1) show only a weight loss (∼2%) at 150−900 °C. In contrast, the TG curves of the modified silica nanoparticles (N2−N4) all show significant weight loss, which is mainly attributed to the introduction of trimethylchlorosilane. For the TG curves of N2, N3, and N4, in the temperature range of 30−300 °C, the weight loss is mainly due to the unreacted reagent or the residual solvents; in the temperature range of 300−700 °C, the weight loss is mainly due to the decomposition of $Si-CH_3$; and in the temperature range of 700−800 °C, the weight loss is because the formation of CH_4 was most probably due to the further reaction of the thermally decomposed product CH_3 with hydroxyl groups on the surface of N2−N4.[30,46] Based on the TGA analysis, we can calculate the amount of methyl groups. According to the TGA results, the $-CH_3$ content of N1−N4 is estimated to be 0, 17, 20, and 25%, respectively. So, we can presume that the hydroxyl content decreases as the methyl content increases.

As the dynamic light scattering (DLS) data show in Figure 1c, the diameters of N0−N4 are 142, 91, 220, 220, and 255 nm, respectively. Scanning electron micrographs (Figure 1d−h) show that these particles are irregular spheres, and the size distributions are wide. Also, similar results can be found in the transmission electron microscopy (TEM) images (Figures 1i−l and S1). These results indicate that the silica particles are a wide distribution in size and the presence of aggregates. In addition, the surface of N0 is folded, and the surface of N1−N4 is smooth, as can be roughly seen from the SEM image. It is further verified by TEM that the surface of N0 has folded pores, and the surface of N1−N4 is flat and smooth (Figures S1 and 1i−l). Despite the absence of folded spaces, the gaps between the heterogeneously sized spheres also have the same high specific surface area and large pore capacity, both of which favor high SP dispersion of the load.

Nitrogen adsorption measurements were carried out and the specific surface areas were calculated using the Brunauer−Emmett−Taylor (BET) method to confirm the ability to load SP. Figures 2 and S2 show the nitrogen adsorption−desorption isotherm of silica nanoparticles with different hydroxyl contents. And the corresponding inset shows the corresponding pore size distribution for N0−N4. As shown in Figures 2a−d and S2a, N0 and N1 exhibit a typical type IV isotherm with a small H-3 hysteresis loop and an H-2 hysteresis loop at a relative pressure (P/P_0) of 0.1−0.9. N2, N3, and N4 all exhibit a type I isotherm with a significant H-4 hysteresis loop at a relative pressure (P/P_0) of 0.1−0.9. This means that the pore sizes and shapes of all samples are widely distributed. According to the classification of pores in the International Union of Pure and Applied Chemistry (IUPAC), N0 and N1 are mesoporous and N2−N4 are micropores. It is noteworthy that N0 is the pore created by the nanoparticle itself due to template agent removal, while N1−N4 have the intermolecular porosity created by the sphere packing. Also, the pore size distribution curves indicate that there is a range of irregular pores in N0−N4, and their optimum pore sizes are 3.5, 6.0, 1.9, 1.9, and 1.9 nm (calculated from the desorption branches), respectively. This indicates that the pore gaps of N2−N4 are more uniformly distributed, which is more favorable to fully dispersing SP molecules.[47,48] The textural parameters derived from the isotherms are provided in Table 1. We can find that

Table 1. Textural Parameters of Silica Nanoparticles Before and After Loading with SP Extracted from Nitrogen Adsorption−Desorption Isotherms in Different Quantities

sample name	S_{BET} (m^2/g)	pore capacity (m^3/g)	pore size (nm)
N0	612	1.3	3.5
N1	352	0.4	6.0
N2	593	0.2	1.9
N3	590	0.2	1.9
N4	205	0.1	1.9
N0@SP	238	1.0	7.7
N1@SP	111	0.2	3.9
N2@SP	268	0.1	1.9
N3@SP	199	0.1	1.9
N4@SP	18	0.0	2.0

the specific surface area (S_{BET}) of N2 and N3 is between those of N0 (612 m^2/g) and N1 (352 m^2/g) and decreases gradually (from 593 to 590 m^2/g), which is due to the gradual increase of methyl content that leads to the decrease of specific surface area. But it is worth noting that the specific surface area of N4 is only 205.4 m^2/g, so if we continue down the list, the specific surface area of the samples will be even smaller and therefore is not conducive to the adsorption of the photochromic dyes, and thus we did not go for much higher density of methyl grafting. In addition, the N0−N4 pore capacity was in the range of 0.1−1.3 m^3/g. We can intuitively analyze that all samples have high S_{BET} and pore capacity, which indicates that they are expected to become matrix substances in adsorbing and storing spiropyran molecules. Certainly, from the pore size data shown in Figures 2a−d and S2a and Table 1, the pore sizes of the samples are between 1 and 6 nm, which is suitable for doping SP (∼5.4 × 5.8 × 11.6 $Å^3$) into silica nanoparticles pore channels. As shown in Figure 2i, spiropyran isomerizes under light stimulation to produce the colored MC form, which has a molecular size of ∼3.6 × 5.6 × 12.9 $Å^3$. It is thus clear that the five silica nanoparticles (N0−N4) also provide sufficient spatial freedom to achieve switching between the SP and MC forms. This is also direct evidence that the prepared silica nanoparticles have sufficient space available for the solid spiropyran to undergo the isomeric process.

https://doi.org/10.1021/acsomega.3c01604
ACS Omega 2023, 8, 16459−16470

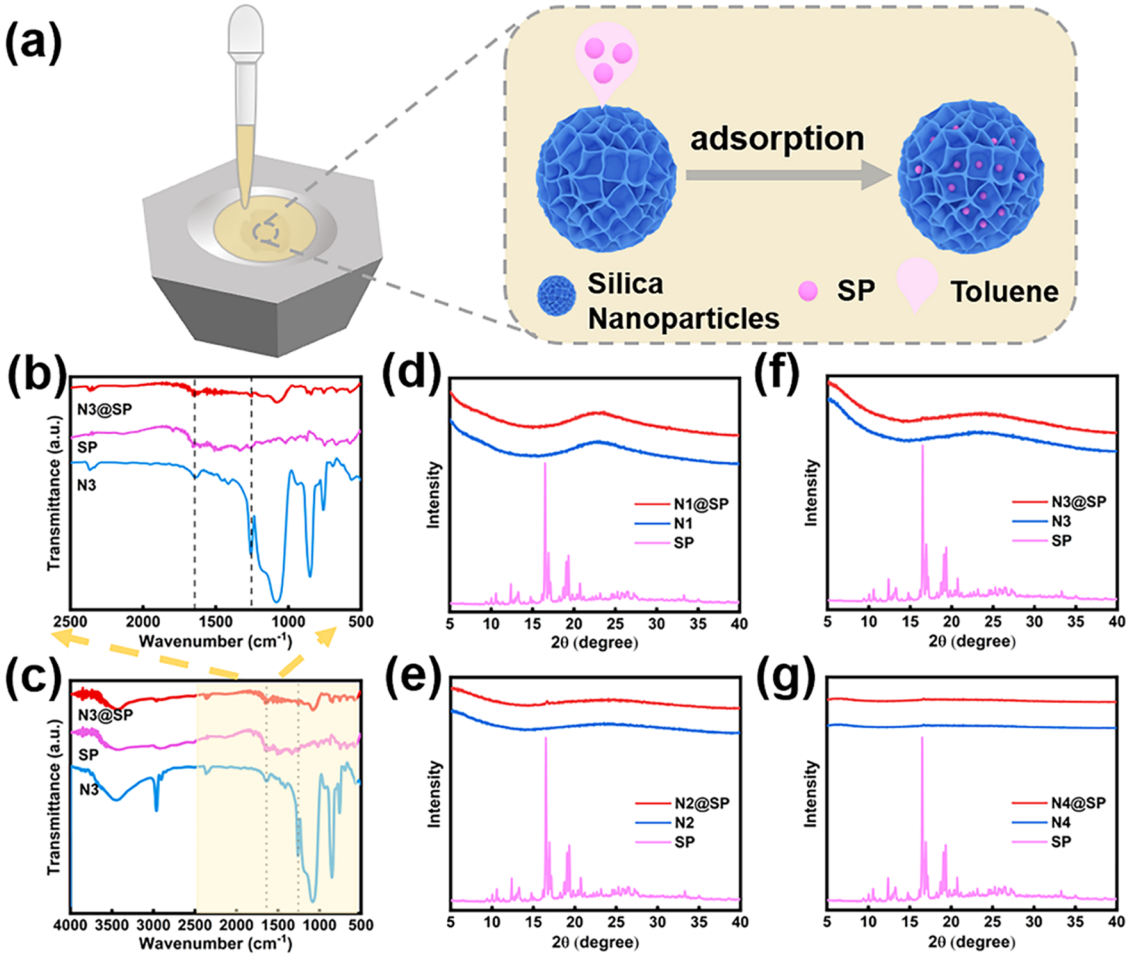

Figure 3. (a) Schematic illustrated the synthesis of SP impregnated in silica nanoparticles. (b) Amplified FT-IR spectra and (c) the FT-IR spectra of N3@SP. The PXRD patterns of (d) N1@SP, (e) N2@SP, (f) N3@SP, and (g) N4@SP.

In order to investigate the effect of the hydroxyl group content of silica on the UV discoloration and visible fading behavior of SP, we prepared a series of complexes by encapsulating SP in functionalized silicas nanoparticles (N0−N4) and further verified whether the loading is successful by FT-IR, powder X-ray diffraction (PXRD), and BET. Figure 3a shows a schematic diagram of the process of silica nanoparticle adsorption of spiropyran. FT-IR tested the complexes (Figures 3b,c and S3a). Taking N3@SP as an example, the characteristic vibrational peaks of the SP molecule are the $-NO_2$ (1650 cm^{-1}) and C−O (1260 cm^{-1}) stretching. The changes of these two characteristic peaks before and after loading were not significant enough to prove the presence or absence of spiropyran in the mixture. Afterward, further analysis of before and after SP doping was performed by PXRD; it was confirmed that the silica nanoparticles (N0−N4) are amorphous porous structures (see Figures S3b and 3d−g blue curves).[43] PXRD measurements further confirmed that the amorphous porous structure of the silica nanopartice hosts was retained after SP incorporation since reflexes from large dye crystals outside the pores were not observed at a higher angle of the 2θ angle. Finally, the mixtures obtained from SP molecules loaded with silica nanoparticles were tested by BET to obtain the nitrogen adsorption and desorption curves and pore size distribution curves in Figures 2e−h and S2b. And the corresponding specific surface area, pore capacity, and pore size are summarized in Table 1. Compared with the preloaded silica nanoparticles, the pore structure of the loaded mixture was unchanged, but there was a significant decrease in specific surface area and pore capacity. Among them, the specific surface area of N0 decreased from 612 to 238 m^2/g, and the pore capacity decreased from 1.3 to 1.0 m^3/g; the specific surface area of N1 decreased from 352 to 111 m^2/g, and the pore capacity decreased from 0.4 to 0.2 m^3/g; the specific surface area of N2 decreased from 593 to 268 m^2/g, and the pore capacity decreased from 0.2 to 0.1 m^3/g; the specific surface area of N3 decreased from 590 to 199 m^2/g, and the pore capacity decreased from 0.2 to 0.1 m^3/g; and the specific surface area of N4 decreased from 205 to 18 m^2/g, and pore capacity decreased from 0.1 to 0.0 m^3/g. It can be seen that the decrease in specific surface area and pore capacity of silica nanoparticles before and after loading is due to the intervention of SP. Therefore, these tests can prove the successful loading of SP molecules.

3.2. Photochromic Properties. Due to incomplete condensation during silica formation, the silica matrix walls of N1 are covered with free silanol groups. Photochromic molecules tend to interact with these silanol groups, thus affecting the light-switching properties. By using TMCS-modified silica, we can reduce the silanol groups, which may have a significant effect on light switching. Therefore, we investigated the photochromic behavior of NX@SP in the powder state. For the N0@SP and N1@SP systems, as shown in Figure S4, no change in UV absorbance was observed under

https://doi.org/10.1021/acsomega.3c01604
ACS Omega 2023, 8, 16459−16470

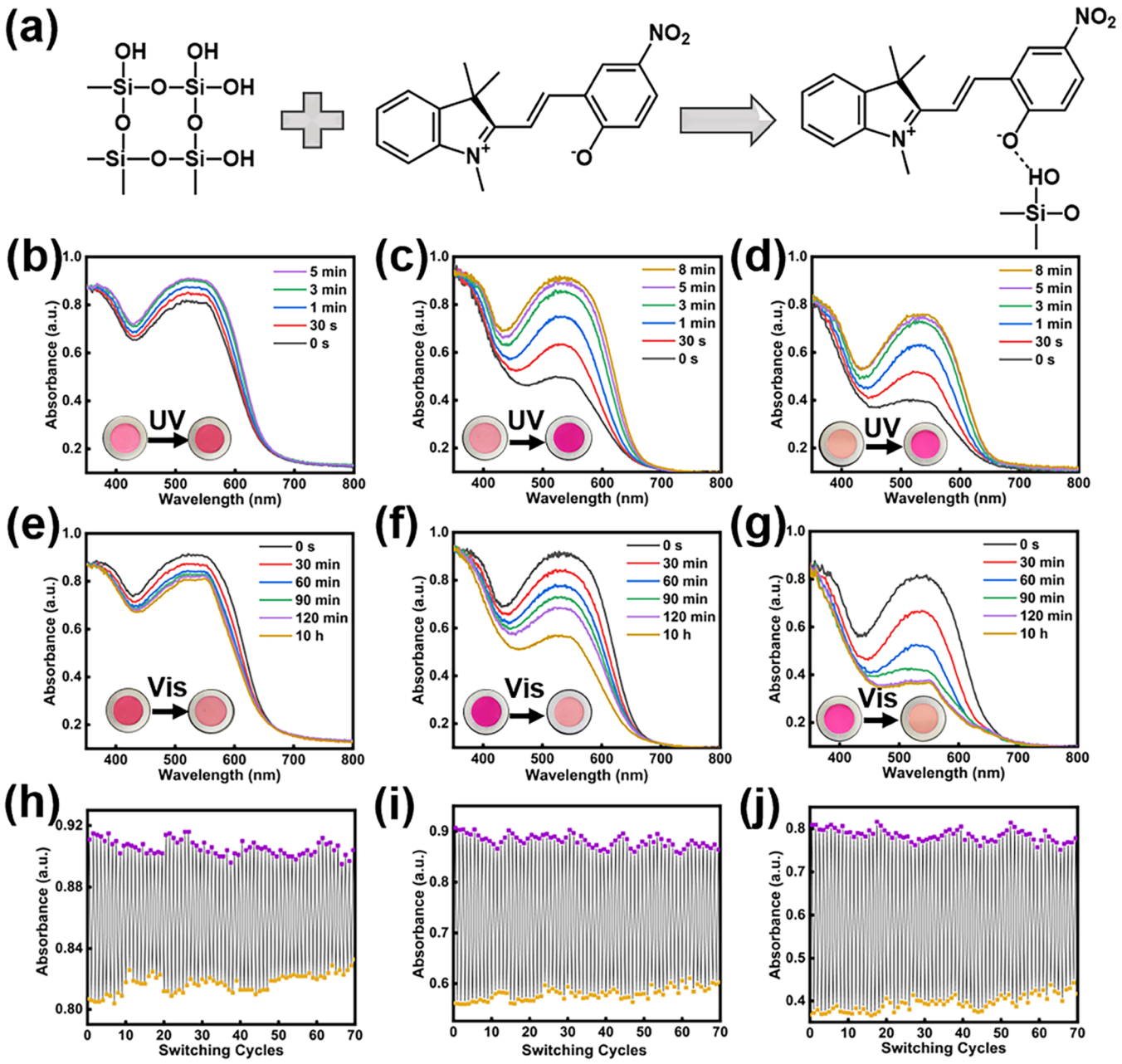

Figure 4. (a) Mechanisms of silanol groups affecting the discoloration of spiropyran. UV−vis absorption spectra of samples with different behavior: (b) N2@SP, (c) N3@SP, and (d) N4@SP correspond to coloration, and (e−g) correspond to their decoloration, respectively (insets: pictures in the lower left corner show the object under UV/vis irradiation). The cycle performance diagram of (h) N2@SP, (i) N3@SP, and (j) N4@SP through 70 cycles of coloring at ultraviolet irradiation and decoloring at visible light.

continuous UV irradiation, indicating that they have no photochromic behavior. According to the literature,[30,43] the absence of photochromic behavior in the N0@SP and N1@SP systems is mainly due to the formation of stable hydrogen bonds between −OH on silica nanoparticles and O^- in the MC form of spiropyran (Figure 4a), resulting in it stable in the MC form, which prevents photochromic behavior within the system. In this regard, we hypothesized that the photochromic behavior could be achieved by reducing the effect of hydrogen bonding through modification by lowering the silanol moiety. Subsequently, the modified silica nanoparticles loaded with SP were further verified to observe the photochromic phenomenon in the presence of reduced silanol groups. Before UV light irradiation, the color of N2@SP, N3@SP, and N4@SP was more shallowed from pink to flesh pink as the content of −OH groups in the matrices decreased. This observation is validated by the UV−vis absorption spectra in Figure 4b−d. For N2@SP, N3@SP, and N4@SP, their initial absorbance values measured at 530 nm without UV irradiation were 0.81, 0.49, and 0.39, respectively, and with increasing UV irradiation time, these samples reached their maximum absorbance at about 5−8 min with absorbance differences of 0.11, 0.40, and 0.44, respectively. With the decrease of hydroxyl content, the initial absorbance value of the N2@SP, N3@SP, and N4@SP composites is getting lower and lower, and the absorbance difference tends to increase. These systems can present obvious photochromic properties with the color changing from pink to rose or red violet after ultraviolet irradiation. And

https://doi.org/10.1021/acsomega.3c01604
ACS Omega 2023, 8, 16459−16470

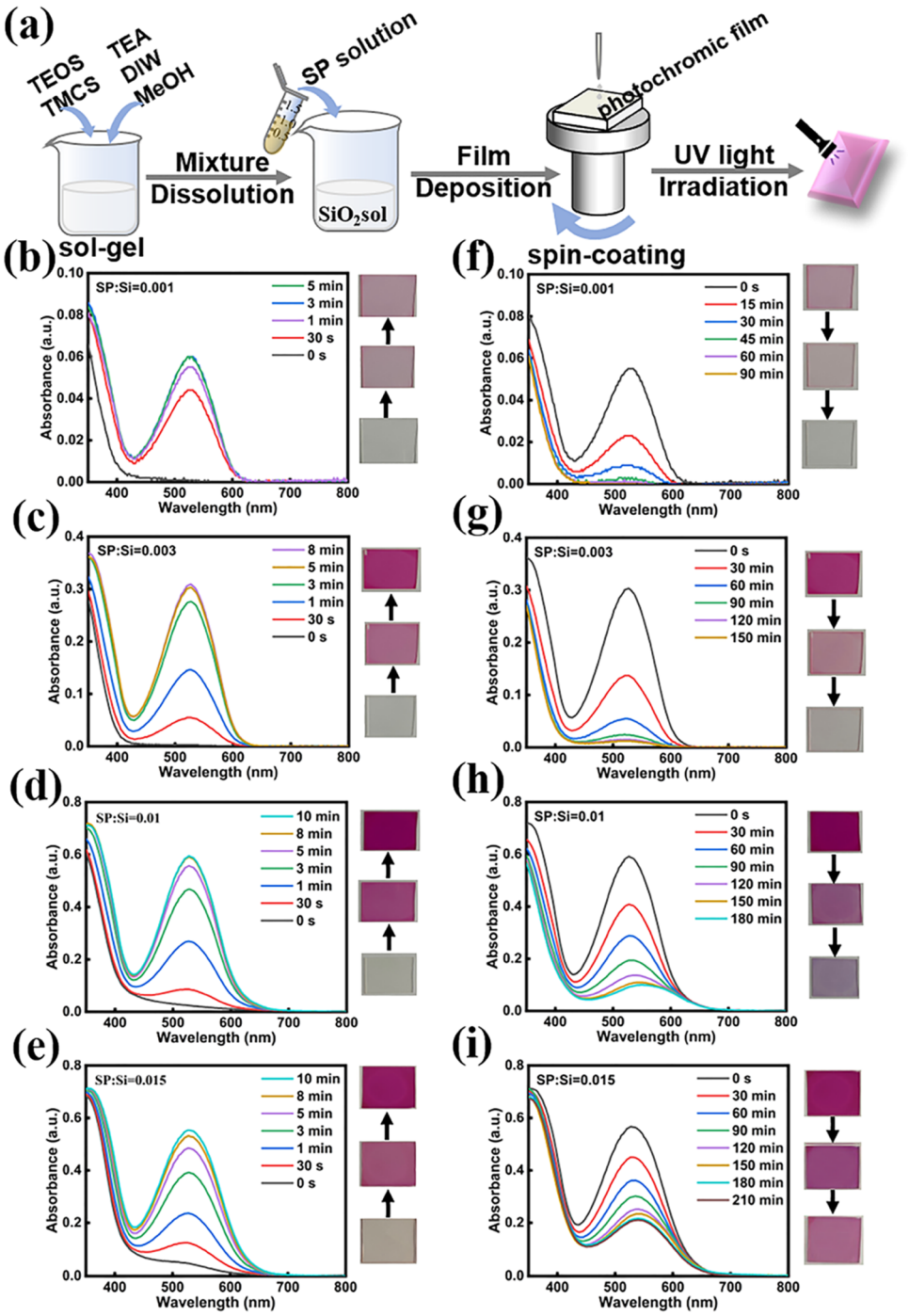

Figure 5. (a) Film-making process. UV−vis absorption spectra of films with different SP/Si ratios by UV/vis stimulation: (b) SP/Si = 0.001, (c) SP/Si = 0.003, (d) SP/Si = 0.01, and (e) SP/Si = 0.015 correspond to UV and (f−i) correspond to their vis, respectively (inset: pictures on the right show the object under UV/vis stimulation).

yet, for the N0@SP and N1@SP systems, before irradiation, all of the SP molecules were in the merocyanine form (MC) but cannot transform back to the SP form even by visible light (Vis) irradiation. For N2@SP, N3@SP, and N4@SP, the UV−vis absorption spectrum before irradiation shows that the higher the density of the Si−CH_3 group of silica, the fewer SP molecules are stabilized by the silica matrix in the merocyanine form (MC) at 530 nm before irradiation. These findings suggest the ability of the surface hydroxyl groups in the silica nanoparticles to hold the spiropyran in the MC state. With increasing UV irradiation time, the intensity of the peak at 530 nm progressively increased, clearly confirming the transition from the SP state to the MC state.

To further verify the photochromic properties and coloring stability of N2@SP, N3@SP, and N4@SP, we investigated their coloring and decolorization processes under UV stimulation and visible light stimulation, respectively. The discoloration and the fading curves could be fitted well by the single-exponential equation (eq 1)

$$\mathrm{Abs}(t) = a e^{-\kappa t} + A_{\infty} \quad (1)$$

https://doi.org/10.1021/acsomega.3c01604
ACS Omega 2023, 8, 16459−16470

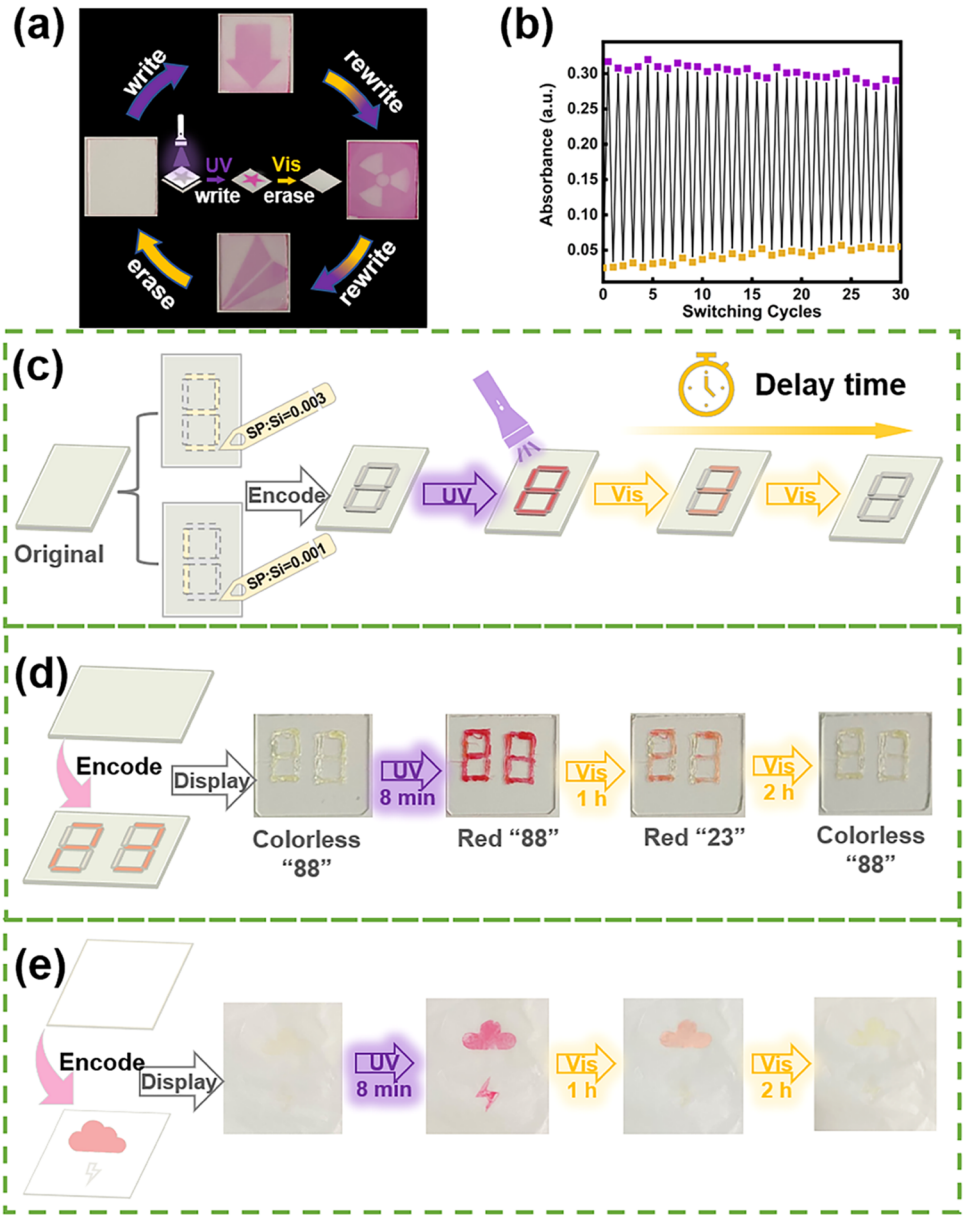

Figure 6. (a) Photochromic film before and after photomask UV writing. Insert: operational approach of optical writing and erasing in the film. (b) Reversible switch of the absorption intensity of the film of SP/Si = 0.003 at 530 nm by alternating UV and vis irradiation. (c) Principal schematic of dynamic anticounterfeiting information. (d) Encrypted message "23" is used for glass. (e) Encryption pattern is used for weighing paper.

where κ is the kinetic constant for discoloration (s^{-1}) and fading (h^{-1}), a is the amplitude, and A_∞ is the residual absorbance. A comparison of the normalized discoloring and fading curves of the powder is shown in Figure S5a,b. The curves in Figure S5a show that N2@SP has the lowest coloring kinetic constant (κ) of 0.0134 s^{-1}, while N4@SP has the highest coloring kinetic constant (0.0164 s^{-1}). The curves in Figure S5b show that N2@SP decolorizes the slowest with the decolorization kinetic constant (κ') of 0.0101 h^{-1}, while N4@SP decolorizes the fastest (0.0135 h^{-1}). It is well known that the solid-state spiropyran photochromic behavior is limited by the space stacking and the polar environment of the substrate material. However, in the present study, we prepared a series of silica nanoparticles with a high specific surface area, large pore capacity, and different polar environments. By comparing their specific surface area and large pore capacity as well as their photochromic behaviors, it can be found that although the specific surface area and pore capacity of N0 are higher than N1, the polar environment is the same, and both exhibit no photochromic behavior. Compared N2, N3 with N4, although the specific surface area and pore capacity of N2 and N3 are higher than N4, N4 is a less polar environment, and the absorbance difference, as well as the coloring and fading ability of N4, were better than those of N2 and N3. Combined, we concluded that N4 has a better photochromic ability and a faster fading rate. The high specific surface area and large pore capacity are favorable conditions for the free space required for the isomerization of spiropyran molecules, but the polar environment created by the silanol groups in silica nanoparticles inhibiting the solid spiropyran photochromic behavior plays an important role. Therefore, as the hydroxyl content in the system decreases, the easier and more rapid the photochromic coloring of the complexes and the more stable the photochromic ability is achieved. In addition, it was also

https://doi.org/10.1021/acsomega.3c01604
ACS Omega 2023, 8, 16459−16470

demonstrated that the hydroxyl group facilitates the stabilization of SP to maintain the MC state, thus reducing the photochromic ability of SP.

3.3. Photochromic Films. Based on NX@SP, the powder is physically adsorbed, which will have certain limitations in the practical application. In order to expand the application field, we use the thin film for further research. The preparation process of the photochromic films is shown in Figure 5a. Through the performance of NX@SP characteristics, we have found that the hydroxyl group of silica stabilizes the spiropyrans within the pores in a colored merocyanine (MC) form (Figure S9). During the preparation of films, we keep the hydroxyl content of the silica pores constant and increase the molar amount of spiropyran molecules inside the pores to regulate the SP/Si molar ratio. In this method, we studied the reversible photochromic properties of the films with different molar ratios of SP/Si. Different from the UV−vis absorption spectra of powders, photochromic films prepared by the sol−gel method have much better reversible properties of color change. The concentration of spiropyran in the matrix is a critical factor in determining the absorption intensity of the film. If significant color changes are to be produced in the film, the requirement for the concentration of photochromic dye is very strict. In addition, adding more spiropyran to the composition will cause the dye to precipitate in the pores, hindering the photochemical ring opening process. Hence, it is very important to optimize the dye concentration according to the overall performance of the photochromic films. In order to find the best reversible photochromic properties, films with different SP/Si mole ratios (0.001, 0.003, 0.01, and 0.015) were prepared. When irradiated with ultraviolet light, all of the obtained samples are dark and show a broad band of around 530 nm (Figure 5b−e). For each film with a different SP/Si molar ratio, with longer UV irradiation times, color changes gradually become obvious, and the maximum absorbance can be reached within 10 min of ultraviolet irradiation. With the increase of SP/Si molar ratio, the absorbance of the photochromic film first increased and then stabilized under the stimulation of UV light, with the color changed from pinkish purple to dark purple. With the SP/Si ratio increased, it was found that the absorbance of the irradiated samples sequentially increased, reaching a saturation value around SP/Si = 0.01 (Figure 5d). According to the UV−vis absorption spectra in Figure 5f−i, it can be obviously seen that the fading time of photochromic films with different SP/Si mole ratios is different. With the increase of SP/Si molar ratios, the fading time of films gradually increased, and even the original color cannot be completely recovered when the SP/Si molar ratios reached 0.015. The reason may be that when spiropyrans are dispersed into the polar silica pores, the influence degree of the OH group on SP molecules is different as the ratio of SP/Si increases. When the ratio of SP/Si is low, SP molecules can move freely in the pores, and the interaction between the MC and OH groups is very weak; only a little MC was stabilized by OH on the silica wall. While as the ratio of SP/Si increased, more SP molecules interacted with the hydroxyl groups, and the stabilized MC forms can hardly return to SP forms, thus leading to a low fading speed. As a result, the spiropyran molecule is in a different polar environment with different molar ratios of SP/Si, which can further prove that the different fading time of the different molar ratios of SP/Si is caused by the polar environment and the result is consistent with the result of the powders.

4. APPLICATION

We obtained reusable photochromic films by coating sol−gel with an SP/Si molar ratio of 0.003. The mask plate with the pattern was placed on top of the film and irradiated with a UV lamp. After removal of the mask, the part protected by the plate remains colorless under the UV lamp, while the exposed part turns red-violet. Finally, a good-looking pattern can be accurately applied to the glass (Figure 6a). What is more, the change from colorless to red-violet is extremely obvious and can be easily distinguished by the naked eye. It can then be completely restored to colorlessness after 2 h of visible light exposure. We then performed fatigue resistance tests on the photochromic films. The thin film maintained good reversible photochromic performance after 30 cycles of switching back and forth between ultraviolet and visible light irradiation (Figure 6b).

In order to explore its promising application in anticounterfeiting, we created a time-dependent anticounterfeiting message using the different fading times of films with different SP/Si molar ratios. The schematic diagram is shown in Figure 6c. We prepare an encrypted message “8” on a substrate using photochromic sols. The message code is composed of two types of sols with SP/Si = 0.001 and SP/Si = 0.003. The main part of “8” is written “3” with the SP/Si = 0.003 sol and “1” with the SP/Si = 0.001 sol. The sol with different SP/Si molar ratios can change color under UV light. However, under the stimulus of visible light, the UV-irradiated sols with SP/Si = 0.003 take longer to fade than the sols with SP/Si = 0.001. Thus, for the encrypted message, it is colorless “8” in its initial state. When the encrypted message is irradiated with UV light for 8 min, it shows a red “8” message. Afterward, when UV light is removed and stimulated by visible light, the encrypted message returns to its original state after changing from “8” to “3” with increasing stimulation time under visible light stimulation. First, we prepare an encrypted message “23” on a glass substrate using the photochromic sols (Figure 6d). The main part of “23” is written with the SP/Si = 0.003 sol and the rest with the SP/Si = 0.001 sol. Thus, for the encrypted message, it is colorless “88” in its initial state. When the encrypted message is irradiated with UV light for 8 min, it shows a fake red “88” message. Afterward, under visible light stimulation, the red “88” turns into pink “23” (true information) when the stimulation time reaches 1 h. After another 1 h, the encrypted message returns to the original colorless “88” message. Further, we used the same encryption to draw the encryption pattern on the weighing paper (Figure 6e). This cryptogram is a symbol for weather, consisting of clouds and lightning, where the clouds are drawn with a sol of SP/Si = 0.003, and the lightning is drawn with a sol of SP/Si = 0.001. In the initial state, there is no pattern displayed on the weighing paper. When UV light is applied to the encrypted pattern for 8 min, a red thunderstorm is displayed on the weighing paper. When the UV light was removed and visible light stimulation was applied, after 1 h, the lightning faded to colorless on the weighing paper, leaving only a pink overcast sky. After a further 1 h, the weighing paper returned to a colorless state. Thus, the sols of photochromic films can adhere to any substrate like glue, which provides a wider range of applications for anticounterfeiting information and avoids the detrimental effects of substrates on anticounterfeiting information. In addition, the fading time of thin films with different SP/Si molar ratios is also different, and time-

https://doi.org/10.1021/acsomega.3c01604
ACS Omega 2023, 8, 16459−16470

dependent information encryption can be prepared by using this difference. As a result, there are potential applications for photochromic films for future anticounterfeiting information and UV printing.

5. CONCLUSIONS

In summary, trimethylchlorosilane has successfully modified the silanol groups of silica nanoparticles and reduced the content of the hydroxyl group of silica. Our experimental results show the same behavior as the work reported by Allouche, which can further demonstrate that it does not make a difference if the responsive molecule is chemically grafted or simply physically attached to the silica nanoparticle surface. In order to enlarge the application of the inorganic−organic hybrid complex, photochromic films were prepared by the sol−gel method. This kind of film not only has excellent photochromic properties but also are colorless in the initial state and can be coated on any external carrier. Notably, these membranes showed excellent fatigue and can be recycled more than 30 times, showing promising applications in anticounterfeiting and UV printing. What is more, the fading time of photochromic films with different SP/Si molar ratios is different, so the composite photochromic films have a dynamic anticounterfeiting effect, which is a good reference for future security anticounterfeiting and information encryption. The invisible ink with time-dependent photochromic performance reported in this paper is expected to improve the level of information security.

■ ASSOCIATED CONTENT

Supporting Information

The Supporting Information is available free of charge at https://pubs.acs.org/doi/10.1021/acsomega.3c01604.

Materials and reagents, characterizations, modification of porous silica nanoparticles (N1−N4), preparations of photochromic the NX@SP complex, preparation of photochromic films, preparation routes of NX@SP, FT-IR spectra of NX@SP powders and SP, UV−vis absorption spectra of N1@SP, and dynamics analysis on powders and films (PDF)

■ AUTHOR INFORMATION

Corresponding Author

Yuhui Yang − *College of Materials Science and Engineering, Zhejiang Sci-Tech University, Hangzhou 310018, China; Department of Polymer Materials and Institute of Smart Biomedical Materials, Zhejiang Sci-Tech University, Hangzhou 310018, China;* orcid.org/0000-0001-7560-5328; Email: yhyang@zstu.edu.cn

Authors

Huimin Zhao − *College of Materials Science and Engineering, Zhejiang Sci-Tech University, Hangzhou 310018, China*

Yuqing Li − *College of Materials Science and Engineering, Zhejiang Sci-Tech University, Hangzhou 310018, China*

Yilong Chen − *College of Materials Science and Engineering, Zhejiang Sci-Tech University, Hangzhou 310018, China*

Zhaohui Wang − *College of Materials Science and Engineering, Zhejiang Sci-Tech University, Hangzhou 310018, China*

Wei Wu − *College of Materials Science and Engineering, Zhejiang Sci-Tech University, Hangzhou 310018, China*

Leilei Hu − *College of Materials Science and Engineering, Zhejiang Sci-Tech University, Hangzhou 310018, China*

Jiangkun Zhu − *College of Materials Science and Engineering, Zhejiang Sci-Tech University, Hangzhou 310018, China*

Complete contact information is available at: https://pubs.acs.org/10.1021/acsomega.3c01604

Author Contributions

‖Y.Y. and H.Z. contributed equally to this work.

Notes

The authors declare no competing financial interest.

■ ACKNOWLEDGMENTS

The authors are grateful for the support provided by the National Natural Science Foundation of China under Grant No. 51803184.

■ REFERENCES

(1) Zhao, S.; Siqueira, G.; Drdova, S.; Norris, D.; Ubert, C.; Bonnin, A.; Galmarini, S.; Ganobjak, M.; Pan, Z.; Brunner, S.; Nystrom, G.; Wang, J.; Koebel, M. M.; Malfait, W. J. Additive manufacturing of silica aerogels. *Nature* **2020**, *584*, 387−392.

(2) Yuan, Y.; Shao, J.; Zhong, M.; Wang, H.; Zhang, C.; Wei, J.; Li, K.; Xu, J.; Zhao, W. Paper Information Recording and Security Protection Using Invisible Ink and Artificial Intelligence. *ACS Appl. Mater. Interfaces* **2021**, *13*, 19443−19449.

(3) Yan, Q.; Wang, S. Fusion of aggregation-induced emission and photochromics for promising photoresponsive smart materials. *Mater. Chem. Front.* **2020**, *4*, 3153−3175.

(4) Wang, L.; Liu, Y.; Zhan, X.; Luo, D.; Sun, X. Photochromic transparent wood for photo-switchable smart window applications. *J. Mater. Chem. C* **2019**, *7*, 8649−8654.

(5) Wang, L.; Feng, J.; Luo, Y.; Zhou, Z.; Jiang, Y.; Luo, X.; Xu, L.; Li, L.; Feng, J. Three-Dimensional-Printed Silica Aerogels for Thermal Insulation by Directly Writing Temperature-Induced Solidifiable Inks. *ACS Appl. Mater. Interfaces* **2021**, *13*, 40964−40975.

(6) Samanta, A.; Chen, H.; Samanta, P.; Popov, S.; Sychugov, I.; Berglund, L. A. Reversible Dual-Stimuli-Responsive Chromic Transparent Wood Biocomposites for Smart Window Applications. *ACS Appl. Mater. Interfaces* **2021**, *13*, 3270−3277.

(7) Mi, R.; Li, T.; Dalgo, D.; Chen, C.; Kuang, Y.; He, S.; Zhao, X.; Xie, W.; Gan, W.; Zhu, J.; Srebric, J.; Yang, R.; Hu, L. A Clear, Strong, and Thermally Insulated Transparent Wood for Energy Efficient Windows. *Adv. Funct. Mater.* **2019**, *30*, No. 1907511.

(8) Ju, H.; Zhu, C. N.; Wang, H.; Page, Z. A.; Wu, Z. L.; Sessler, J. L.; Huang, F. Paper without a Trail: Time-Dependent Encryption using Pillar[5] arene-Based Host-Guest Invisible Ink. *Adv. Mater.* **2022**, *34*, No. 2108163.

(9) Huang, Y.; Bisoyi, H. K.; Huang, S.; Wang, M.; Chen, X. M.; Liu, Z.; Yang, H.; Li, Q. Bioinspired Synergistic Photochromic Luminescence and Programmable Liquid Crystal Actuators. *Angew. Chem., Int. Ed.* **2021**, *60*, 11247−11251.

(10) Han, F.; Wang, T.; Lium, G.; Liu, H.; Xie, X.; Wei, Z.; Li, J.; Jiang, C.; He, Y.; Xu, F. Materials with Tunable Optical Properties for Wearable Epidermal Sensing in Health Monitoring. *Adv. Mater.* **2022**, *34*, No. 2109055.

(11) Du, Z.; Zhang, T.; Gai, H.; Sheng, L.; Guan, Y.; Wang, X.; Qin, T.; Li, M.; Wang, S.; Zhang, Y. M.; Nie, H.; Zhang, S. X. Multi-Component Collaborative Step-by-Step Coloring Strategy to Achieve High-Performance Light-Responsive Color-Switching. *Adv. Sci.* **2022**, *9*, No. 2103309.

(12) Kortekaas, L.; Browne, W. R. The evolution of spiropyran: fundamentals and progress of an extraordinarily versatile photochrome. *Chem. Soc. Rev.* **2019**, *48*, 3406−3424.

(13) Dridi, H.; Boulmier, A.; Bolle, P.; Dolbecq, A.; Rebilly, J.-N.; Banse, F.; Ruhlmann, L.; Serier-Brault, H.; Dessapt, R.; Mialane, P.;

Oms, O. Directing the solid-state photochromic and luminescent behaviors of spiromolecules with Dawson and Anderson polyoxometalate units. *J. Mater. Chem. C* **2020**, *8*, 637−649.
(14) Yonekawa, I.; Mutoh, K.; Kobayashi, Y.; Abe, J. Intensity-Dependent Photoresponse of Biphotochromic Molecule Composed of a Negative and a Positive Photochromic Unit. *J. Am. Chem. Soc.* **2018**, *140*, 1091−1097.
(15) Feeney, M. J.; Thomas, S. W. Tuning the Negative Photochromism of Water-Soluble Spiropyran Polymers. *Macromolecules* **2018**, *51*, 8027−8037.
(16) Qiu, W.; Gurr, P. A.; Qiao, G. G. Color-Switchable Polar Polymeric Materials. *ACS Appl. Mater. Interfaces* **2019**, *11*, 29268−29275.
(17) Sun, F.; Wang, D. Toward real-world applications: promoting fast and efficient photoswitching in the solid state. *J. Mater. Chem. C* **2022**, *10*, 13700−13716.
(18) Shiraishi, Y.; Adachi, K.; Itoh, M.; Hirai, T. Spiropyran as a Selective, Sensitive, and Reproducible Cyanide Anion Receptor. *Org. Lett.* **2009**, *11*, 3482−3485.
(19) Abdollahi, A.; Roghani-Mamaqani, H.; Razavi, B. Stimuli-chromism of photoswitches in smart polymers: Recent advances and applications as chemosensors. *Prog. Polym. Sci.* **2019**, *98*, No. 101149.
(20) Hou, I. C.; Berger, F.; Narita, A.; Mullen, K.; Hecht, S. Proton-Gated Ring-Closure of a Negative Photochromic Azulene-Based Diarylethene. *Angew. Chem., Int. Ed.* **2020**, *59*, 18532−18536.
(21) Li, S.; Li, M.; Chen, L.; Yang, J.; Wang, Z.; Yang, F.; He, L.; Li, X. Engineering highly efficient Li^+ responsive nanochannels via host-guest interaction and photochemistry regulation. *J. Colloid Interface Sci.* **2022**, *615*, 674−684.
(22) Meeks, A.; Lerch, M. M.; Schroeder, T. B. H.; Shastri, A.; Aizenberg, J. Spiropyran Photoisomerization Dynamics in Multi-responsive Hydrogels. *J. Am. Chem. Soc.* **2022**, *144*, 219−227.
(23) Otaegui, J. R.; Ruiz-Molina, D.; Latterini, L.; Hernando, J.; Roscini, C. Thermoresponsive multicolor-emissive materials based on solid lipid nanoparticles. *Mater. Horiz.* **2021**, *8*, 3043−3054.
(24) Qiu, W.; Gurr, P. A.; da Silva, G.; Qiao, G. G. Insights into the mechanochromism of spiropyran elastomers. *Polym. Chem.* **2019**, *10*, 1650−1659.
(25) Yu, X.; Wu, L.; Yang, D.; Cao, M.; Fan, X.; Lin, H.; Zhong, Q.; Xu, Y.; Zhang, Q. Hydrochromic CsPbBr3 Nanocrystals for Anti-Counterfeiting. *Angew. Chem., Int. Ed.* **2020**, *59*, 14527−14532.
(26) Yang, Z.; Wang, D.; Zhang, Y.; Feng, Z.; Liu, L.; Wang, W. Photoreductive BiOCl Ultrathin Nanosheets for Highly Efficient Photocatalytic Color Switching. *ACS Appl. Mater. Interfaces* **2020**, *12*, 8604−8613.
(27) Carroli, M.; Duong, D. T.; Buchaca-Domingo, E.; Liscio, A.; Börjesson, K.; Herder, M.; Palermo, V.; Hecht, S.; Stingelin, N.; Salleo, A.; Orgiu, E.; Samorì, P. The Role of Morphology in Optically Switchable Transistors Based on a Photochromic Molecule/p-Type Polymer Semiconductor Blend. *Adv. Funct. Mater.* **2019**, *30*, No. 1907507.
(28) Abdollahi, A.; Alidaei-Sharif, H.; Roghani-Mamaqani, H.; Herizchi, A. Photoswitchable fluorescent polymer nanoparticles as high-security anticounterfeiting materials for authentication and optical patterning. *J. Mater. Chem. C* **2020**, *8*, 5476−5493.
(29) Santiago, S.; Gimenez-Gomez, P.; Munoz-Berbel, X.; Hernando, J.; Guirado, G. Solid Multiresponsive Materials Based on Nitrospiropyran-Doped Ionogels. *ACS Appl. Mater. Interfaces* **2021**, *13*, 26461−26471.
(30) Pinto, T. V.; Costa, P.; Sousa, C. M.; Sousa, C. A.; Monteiro, A.; Pereira, C.; Soares, O. S.; Silva, C. S.; Pereira, M. F.; Coelho, P. J.; Freire, C. Naphthopyran-Based Silica Nanoparticles as New High-Performance Photoresponsive Materials. *ACS Appl. Mater. Interfaces* **2016**, *8*, 7221−7231.
(31) Pardo, R.; Zayat, M.; Levy, D. Thin film photochromic materials: Effect of the sol-gel ormosil matrix on the photochromic properties of naphthopyrans. *C. R. Chim.* **2010**, *13*, 212−226.
(32) Chu, Z.; Klajn, R. Polysilsesquioxane Nanowire Networks as an "Artificial Solvent" for Reversible Operation of Photochromic Molecules. *Nano Lett.* **2019**, *19*, 7106−7111.
(33) Li, Z.; Wang, G.; Ye, Y.; Li, B.; Li, H.; Chen, B. Loading Photochromic Molecules into a Luminescent Metal-Organic Framework for Information Anticounterfeiting. *Angew. Chem., Int. Ed.* **2019**, *58*, 18025−18031.
(34) Zheng, Y.; Sato, H.; Wu, P.; Jeon, H. J.; Matsuda, R.; Kitagawa, S. Flexible interlocked porous frameworks allow quantitative photoisomerization in a crystalline solid. *Nat. Commun.* **2017**, *8*, No. 100.
(35) Allouche, J.; Le Beulze, A.; Dupin, J.-C.; Ledeuil, J.-B.; Blanc, S.; Gonbeau, D. Hybrid spiropyran−silica nanoparticles with a core-shell structure: sol−gel synthesis and photochromic properties. *J. Mater. Chem.* **2010**, *20*, 9370−9378.
(36) Pinto, T. V.; Costa, P.; Sousa, C. A.; et al. Screen-Printed Photochromic Textiles through New Inks Based on SiO_2@naphthopyran Nanoparticles. *ACS Appl. Mater. Interfaces* **2016**, *8*, 28935−28945.
(37) Yamaguchi, T.; Maity, A.; et al. Negative Photochromism Based on Molecular Diffusion between Hydrophilic and Hydrophobic Particles in the Solid State. *Inorg. Chem.* **2018**, *57*, 3671−3674.
(38) Liu, X. F.; Zou, L.; Yang, C.; Zhao, W.; Li, X. Y.; Sun, B.; Hu, C. X.; Yu, Y.; Wang, Q.; Zhao, Q.; Zhang, H. L. Fluorescence Lifetime-Tunable Water-Resistant Perovskite Quantum Dots for Multidimensional Encryption. *ACS Appl. Mater. Interfaces* **2020**, *12*, 43073−43082.
(39) Yang, Y.; Li, Y.; Chen, Y.; Wang, Z.; He, Z.; He, J.; Zhao, H. Dynamic Anticounterfeiting Through Novel Photochromic Spiropyran-Based Switch@Ln-MOF Composites. *ACS Appl. Mater. Interfaces* **2022**, *14*, 21330−21339.
(40) Wang, Q.; Zhang, Q.; Zhang, Q. W.; Li, X.; Zhao, C. X.; Xu, T. Y.; Qu, D. H.; Tian, H. Color-tunable single-fluorophore supramolecular system with assembly-encoded emission. *Nat. Commun.* **2020**, *11*, No. 158.
(41) Le, X.; Shang, H.; Wu, S.; Zhang, J.; Liu, M.; Zheng, Y.; Chen, T. Heterogeneous Fluorescent Organohydrogel Enables Dynamic Anti-Counterfeiting. *Adv. Funct. Mater.* **2021**, *31*, No. 2108365.
(42) Zucchetto, N.; Brühwiler, D. Strategies for Localizing Multiple Functional Groups in Mesoporous Silica Particles through a One-Pot Synthesis. *Chem. Mater.* **2018**, *30*, 7280−7286.
(43) Mühlstein, L. A.; Sauer, J.; Bein, T. Tuning the Thermal Relaxation of a Photochromic Dye in Functionalized Mesoporous Silica. *Adv. Funct. Mater.* **2009**, *19*, 2027−2037.
(44) Michailidis, M.; Sorzabal-Bellido, I.; Adamidou, E. A.; Diaz-Fernandez, Y. A.; Aveyard, J.; Wengier, R.; Grigoriev, D.; Raval, R.; Benayahu, Y.; D'Sa, R. A.; Shchukin, D. Modified Mesoporous Silica Nanoparticles with a Dual Synergetic Antibacterial Effect. *ACS Appl. Mater. Interfaces* **2017**, *9*, 38364−38372.
(45) Jiang, J.; Wang, W.; Shen, H.; Wang, J.; Cao, J. Characterization of silica particles modified with γ-methacryloxypropyltrimethoxysilane. *Appl. Surf. Sci.* **2017**, *397*, 104−111.
(46) Jiang, P.; Ma, L.; Pan, J.; Chun, Y.; Xu, Q. H.; Dong, Jl. Preparation of Amphiphilic HZSM-5 Zeolite by Chemical Vapor Deposition of Trimethylchlorosilane. *Chin. J. Catal.* **2009**, *30*, 503−508.
(47) Li, N.; Guo, R.; Oechsle, A. L.; Reus, M. A.; Liang, S.; Song, L.; Wang, K.; Yang, D.; Allegretti, F.; Kumar, A.; Nuber, M.; Berger, J.; Bernstorff, S.; Iglev, H.; Hauer, J.; Fischer, R. A.; Barth, J. V.; Müller-Buschbaum, P. Operando Study of Structure Degradation in Solid-State Dye-Sensitized Solar Cells with a TiO_2 Photoanode Having Ordered Mesopore Arrays. *Sol. RRL* **2022**, *6*, No. 2200373.
(48) Song, L.; Wang, W.; Körstgens, V.; González, D. M.; Yao, Y.; Minar, N. K.; Feckl, J. M.; Peters, K.; Bein, T.; Fattakhova-Rohlfing, D.; Santoro, G.; Roth, S. V.; Müller-Buschbaum, P. Spray Deposition of Titania Films with Incorporated Crystalline Nanoparticles for All-Solid-State Dye-Sensitized Solar Cells Using P3HT. *Adv. Funct. Mater.* **2016**, *26*, 1498−1506.

https://doi.org/10.1021/acsomega.3c01604
ACS Omega 2023, 8, 16459−16470